Models of quantum tunneling of a diatomic molecule affected by laser pulses through repulsive barriers

S. Vinitsky[a], A. Gusev[a], O. Chuluunbaatar[a], L.L. Hai[a], V. Derbov[b], P.M. Krassovitskiy[c]

[a]Joint Institute for Nuclear Research, 6 Joliot-Curie St., 141980, Dubna, Moscow region, Russia;

[b]Saratov State University, 83 Astrakhanskaya St., Saratov, 410012, Russia;

[c]Institute of Nuclear Physics, 1 Ibragimov St., Almaty, 050032, Kazakhstan.

ABSTRACT

The model for quantum tunneling of a diatomic homonuclear molecule is formulated as a 2D boundary-value problem (2D BVP) for the Schrödinger equation with homogeneous boundary conditions of the third type. The molecule is considered as a pair of identical particles coupled via the effective potential. For short-range barrier potentials the Galerkin reduction to BVP for a set of closed-channel second-order ordinary differential equations (ODEs) is obtained by expanding the solution in a basis of transverse variable functions. Benchmark calculations of quantum tunneling through Gaussian barriers are presented for a pair of identical nuclei coupled by Morse potential. The results are compared with the direct numerical solution of the original 2D BVP obtained using the Numerov scheme. The effect of quantum transparency, i.e., the resonance behavior of the transmission coefficient versus the energy of the molecule, is shown to be a manifestation of the barrier metastable states, embedded in the continuum below the dissociation threshold, as well as quantum diffusion. The possibility of controlling the dynamics of atom-ion collisions by laser pulses is analyzed using a 1D BVP two-center model with Pöschl-Teller potentials.

Keywords: tunneling, interatomic potentials, diatomic molecules, quantum diffusion, laser pulses, time-dependent Scrödinger equation

1. INTRODUCTION

The study of tunneling coupled particles through repulsive barriers[1] has revealed the effect of resonance quantum transparency: when the cluster size is comparable with the spatial width of the barrier, there are mechanisms that lead to greater transparency of the barrier. These mechanisms are related to the formation of the barrier resonances, provided that the potential energy of the composite system has local minima giving rise to metastable states of the moving cluster.[2] Currently this effect and its possible applications are a subject of extensive study in relation with different quantum-physical problems, e.g., sub-barrier tunneling of light nuclei,[3] quantum diffusion of molecules,[4] exciton resonance passage through a quantum heterostructure barrier,[5] resonant formation of molecules from individual atoms,[6] controlling the direction of diffusion in solids,[7] and tunnelling of ions and clusters through repulsive barriers.[8,9] One more important problem is the possibility to control the tunneling of molecules by means of laser pulses, which can allow the enhancement of desired chemical reactions.[10] For the analysis of these effects it is useful to develop model approaches based on approximations, providing a realistic description of interactions between the atoms in the molecule, as well as with the barriers and/or external fields.

In this paper we formulate and study the model of a diatomic molecule with the nuclei coupled via the effective Morse potential, tunneling through a Gaussian repulsive barrier. We present the comparison of the close-coupling approximate results with those of the direct numerical solution of the original 2D BVP using the Numerov scheme below the dissociation threshold. The effect of quantum transparency, i.e., the resonance behavior of the transmission coefficient versus the energy of the molecule, as well as quantum diffusion are analyzed. Atom-ion collisions, as well as the dynamics of an ion in the field of a laser pulse, are studied on the base of a two-center model with Pöschl-Teller potentials.

Further author information: (Send correspondence to A.G.)
A.G.: E-mail: gooseff@jinr.ru
S.V.: E-mail: vinitsky@theor.jinr.ru

Saratov Fall Meeting 2013: Optical Technologies in Biophysics and Medicine XV; and Laser Physics and Photonics XV, edited by Elina A. Genina, Vladimir L. Derbov, Igor Meglinski, Valery V. Tuchin, Proc. of SPIE Vol. 9031, 90311D

2. MODEL I. TRANSMISSION OF A DIATOMIC MOLECULE THROUGH A BARRIER

We consider a 2D model of two identical particles with mass m, coupled by pair interaction $\tilde{V}(x_2 - x_1)$ and interacting with barrier potentials $\tilde{V}_b(x_1)$ and $\tilde{V}_b(x_2)$. The relevant stationary Schrödinger equation for the wave function $\Psi(x_1, x_2)$ in the s-wave approximation has the form:

$$\left(\frac{\hbar^2}{2m}\frac{\partial^2}{\partial x_1^2} - \frac{\hbar^2}{2m}\frac{\partial^2}{\partial x_2^2} + \tilde{V}(x_2 - x_1) + \tilde{V}_b(x_1) + \tilde{V}_b(x_2) - \tilde{E}\right)\Psi(x_1, x_2) = 0, \tag{1}$$

where $\tilde{E}$ is total energy of the system and $\hbar$ is Plank constant. Using the change of variables $x = x_2 - x_1$, $y = x_2 + x_1$, we can rewrite Eq. (1) in the form

$$\left(-\frac{\hbar^2}{m}\frac{\partial^2}{\partial y^2} - \frac{\hbar^2}{m}\frac{\partial^2}{\partial x^2} + \tilde{V}(x) + \tilde{V}_b(\frac{x+y}{2}) + \tilde{V}_b(\frac{x-y}{2}) - \tilde{E}\right)\Psi(y, x) = 0. \tag{2}$$

The equation describing the molecular subsystem has the form

$$\left(-\frac{\hbar^2}{m}\frac{d^2}{dx^2} + \tilde{V}(x) - \tilde{\varepsilon}\right)\phi(x) = 0. \tag{3}$$

The molecular subsystem considered is assumed to possess the continuous energy spectrum with the eigenvalues $\tilde{\varepsilon} \geq 0$ and eigenfunctions $\phi_{\tilde{\varepsilon}}(x)$ and the discrete energy spectrum with the finite number n of bound states with the eigenfunctions $\phi_j(x)$ and the eigenvalues $\tilde{\varepsilon}_j = -|\tilde{\varepsilon}_j|$, $j = 1, n$.

The asymptotic boundary conditions imposed on the solution for the 2D model in the s-wave approximation $\Psi(y, x) = \{\Psi_j(y, x)\}_{j=1}^{N_o}$ with the direction $v = \rightarrow$ can be written in the obvious form

$$\begin{aligned}
&\Psi_j(y \to -\infty, x) \to \phi_j(x)\frac{\exp(\imath k_j y)}{\sqrt{k_j}} + \sum_{l=1}^{N_o}\phi_l(x)\frac{\exp(-\imath k_l y)}{\sqrt{k_l}}R_{lj},\\
&\Psi_j(y \to +\infty, x) \to \sum_{l=1}^{N_o}\phi_l(x)\frac{\exp(\imath k_l y)}{\sqrt{k_l}}T_{lj},\\
&\Psi_j(y, x \to \pm\infty) \to 0,
\end{aligned} \tag{4}$$

where R_{lj} and T_{lj} are the reflection and transmission amplitudes, N_o is the number of open channels, k_i is the wave number, $k_i = \sqrt{(m/\hbar^2)(\tilde{E} - \tilde{\varepsilon}_i)} > 0$, below dissociation threshold $\tilde{E} < 0$, $\phi_i(x)$ and ε_i are the eigenfunctions and eigenvalues of the BVP for Eq. (3).

The solution of Eq. (2) is sought for in the form of Galerkin expansion

$$\Psi(y, r) = \sum_{j=1}^{j_{\max}}\phi_j(r)\chi_{ji_o}(y), \tag{5}$$

Here $\chi_{ji_o}(y)$ are unknown functions and the orthonormalized basis functions $\phi_j(r)$ in the interval $0 \leq r \leq r_{\max}$ are defined as eigenfunctions of the BVP for the equation

$$\left(-\frac{d^2}{dr^2} + V(r) - \varepsilon_j\right)\phi_j(r) = 0, \quad \phi_j(0) = \phi_j(r_{\max}) = 0, \quad \int_0^{r_{\max}} dr\phi_i(r)\phi_j(r) = \delta_{ij}, \tag{6}$$

where $V(r) = (m/\hbar^2)\tilde{V}(x)$, $\varepsilon_j = (m/\hbar^2)\tilde{\varepsilon}_j$. The desirable set of numerical solutions of this BVP is calculated with the given accuracy by means of the program ODPEVP.[11] Hence, we calculate the set of n bound states having the eigenfunctions $\phi_j(x)$ and the eigenvalues ε_j, $j = 1, n$ and the desirable set of pseudostates with the eigenfunctions $\phi_j(x)$ and the eigenvalues $\varepsilon_j \geq 0$, $j = n+1, j_{\max}$. The latter approximate the set of continuum eigensolutions $\varepsilon \geq 0$ of the BVP for Eq. (3).

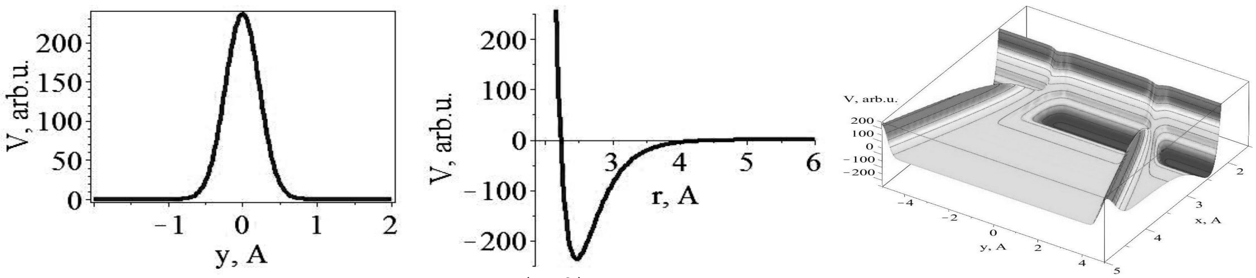

Figure 1. Gaussian-type barrier $V_b(x_i) = \hat{D}\exp\left(-\frac{x_i^2}{2\sigma}\right)$, at $\hat{D} = 236.510003758401\text{Å}^{-2} = (m/\hbar^2)\tilde{V}_0 = (m/\hbar^2)D$, $\tilde{V}_0 = D = 1280\text{K}$, $\sigma = 5.23 \cdot 10^{-2}\text{Å}^2$, the two-particle interaction potential, $V(r) = \hat{D}\{\exp[-2(r-\hat{r}_{eq})\hat{\rho}] - 2\exp[-(r-\hat{r}_{eq})\hat{\rho}]\}$, $\hat{r}_{eq} = 2.47\text{Å}$, $\hat{\rho} = 2.96812423381643\text{Å}^{-1}$ and the corresponding 2D potential.

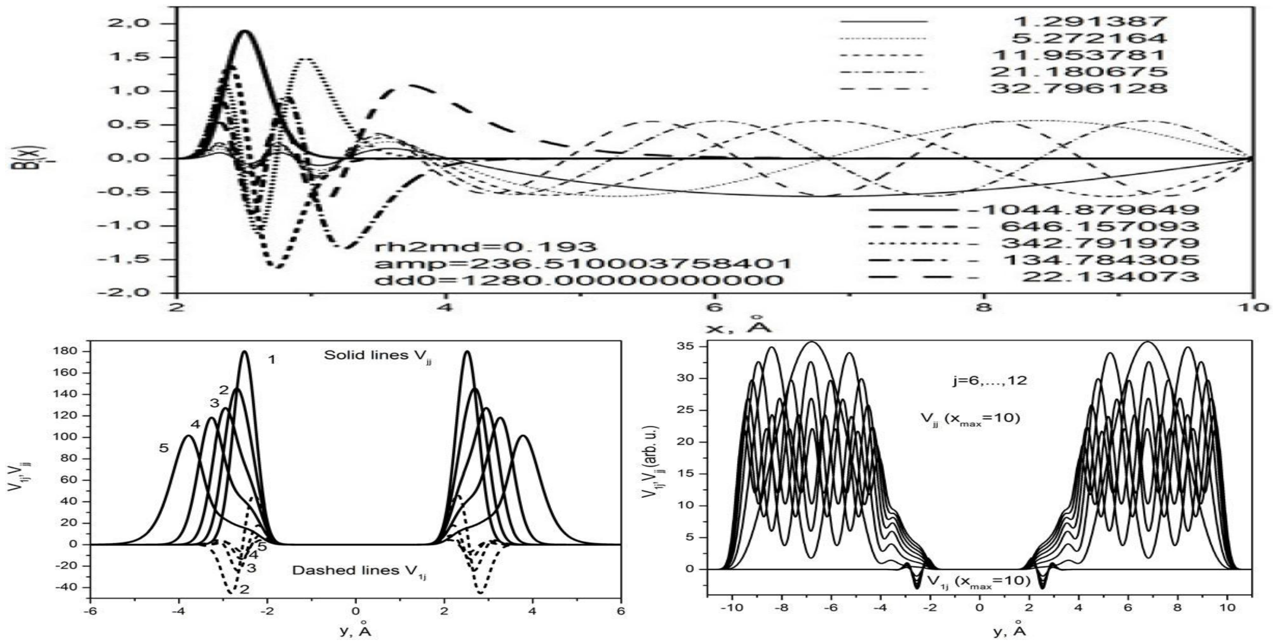

Figure 2. The wave functions $\phi_j(r)$ of the bound states $j = 1, 5$ (solid lines) and pseudostates $j = 6, ..., 15$ (dashed lines) The matrix elements $V_{jj}(y)$ (solid lines) and $V_{j1}(y)$ (dashed lines).

The set of closed-channel Galerkin equations has the form

$$\left[-\frac{d^2}{dy^2} + \varepsilon_i - E\right]\chi_{ii_o}(y) + \sum_{j=1}^{j_{\max}} V_{ij}(y)\chi_{ji_o}(y) = 0. \tag{7}$$

Thus, the scattering problem (2)–(3) with the asymptotic boundary conditions (4) is reduced to the boundary-value problem for the set of close-coupling equations in the Galerkin form (7) with the boundary conditions at $y = y_{\min}$ and $y = y_{\max}$ (from ref.[9]):

$$\left.\frac{d\boldsymbol{F}(y)}{dy}\right|_{y=y_{\min}} = \mathcal{R}(y_{\min})\boldsymbol{F}(y_{\min}),\ \left.\frac{d\boldsymbol{F}(y)}{dy}\right|_{y=y_{\max}} = \mathcal{R}(y_{\max})\boldsymbol{F}(y_{\max}), \tag{8}$$

where $\mathcal{R}(y)$ is an unknown $j_{\max} \times j_{\max}$ matrix function, $\boldsymbol{F}(y) = \{\boldsymbol{\chi}_{i_o}(y)\}_{i_o=1}^{N_o} = \{\{\chi_{ji_o}(y)\}_{j=1}^{j_{\max}}\}_{i_o=1}^{N_o}$ is the required $j_{\max} \times N_o$ matrix solution, and N_o is the number of open channels, $N_o = \max_{E \geq \varepsilon_j} j \leq j_{\max}$, calculated using the third version of the program KANTBP.[12]

In Eq. (7) the effective potentials $V_{ij}(y)$ are expressed by the integrals

$$V_{ij}(y) = \int_0^{r_{\max}} dr \phi_i(r)(V_b(\frac{r+y}{2}) + V_b(\frac{r-y}{2}))\phi_j(r). \quad (9)$$

For example let us take the parameters of the molecule Be_2, namely, the reduced mass $\mu = m/2 = 4.506$Da, the average distance between the atoms 2.47Å, the frequency of molecular vibrations expressed in temperature units $\hbar\omega = 398.72$K, the ground state of molecule $^1\Sigma_u^+$, the wave number of the order of 277.124cm^{-1} for the observable excited-to-ground state transitions (we use relationship 1K= 0.69503476cm^{-1} from[13]). These values were used to determine the parameters of the Morse potential

$$\tilde{V} = D\{\exp[-2(r-\hat{r}_{eq})\hat{\rho}] - 2\exp[-(r-\hat{r}_{eq})\hat{\rho}]\}, \quad (10)$$

where D is the depth of the interaction potential well and $\hat{\rho}$ describes the width of the potential well. The values of D and $\hat{\rho}$ are determined from the known spectrum

$$-\tilde{\varepsilon}_n = D\left[1 - \varsigma(n+1/2)\right]^2. \quad (11)$$

Having the average size of the molecule and the separation between the energy levels taken into account, one can parametrize the molecular potential to fit the observable quantities, namely, $D = 1280$K, $\hat{r}_{eq} = 2.47$Å, $\hat{\rho} = 2.968\text{Å}^{-1}$ is determined from the condition $(\tilde{\varepsilon}_2 - \tilde{\varepsilon}_1)/(2\pi\hbar c) = 277.124\text{cm}^{-1}$, at $\varsigma = \frac{\hat{\rho}\hbar}{\sqrt{mD}} = 0.193$ is the dimensionless constant of the problem and $\hat{D} = (\frac{\sqrt{mD}}{\hbar})^2 = (\hat{\rho}/0.193)^2 = (2.968\text{Å}^{-1}/0.193)^2 = 236.5\text{Å}^{-2}$. In accordance with (11), the ground state energy of the molecule Be_2 is equal to $-\tilde{\varepsilon}_n = -1044.88$K. Since the bond in the molecule Be_2 is of the Van der Waals type, one can consider each constituent atom independently interacting with the external barrier potential. The latter should be chosen to have the height and the width typical for barriers in a real crystal lattice. Moreover, this potential should be a smooth function having the second derivative to apply high-accuracy numerical methods, like the Numerov method or the finite element method, for solving the BVP for the systems of second-order ordinary differential equations. Therefore, we choose the Gaussian repulsive barrier potential

$$\tilde{V}_b(x_i) = \tilde{V}_0 \exp\left(-\frac{x_i^2}{2\sigma}\right), \quad V_b(x_i) = \frac{m}{\hbar^2}\tilde{V}_b(x_i) = \hat{D}\exp\left(-\frac{x_i^2}{2\sigma}\right). \quad (12)$$

Here the parameters $\tilde{V}_0 = 1280K$, $\hat{D} = 236.510003758401\text{Å}^{-2} = (m/\hbar^2)\tilde{V}_0$, $\sigma = 5.23 \cdot 10^{-2}\text{Å}^2$ are determined by the model requirement that the width of repulsive potential at the kinetic energy equal to that of the ground state is 1Å, so that the average distance 2.47Å between the atoms of Be is less that the distance 2.56Åbetween Cu atoms in the plane (111) of the crystal lattice cell. The potential barrier height $\tilde{V}_0$ of the order of 200 meV was estimated following the experimental observation of quantum diffusion of hydrogen atoms.[14] Fig. 1 illustrates the Gaussian and Morse potentials, and the corresponding 2D potential. Fig. 2 presents the calculated eigenfunctions of the BVP (6) and the effective potentials $V_{ij}(y)$ of Eq. (9), calculated using these functions. Note, that the wave functions $\phi_j(r)$ and the eigenvalues $\varepsilon_j(r)$ of the bound states $j = 1, 5$ (solid lines) approximate the known analytical ones of the BVP for Eq. (3) with the Morse potential (10) with four and seven significant digits, respectively, the states being localized in the well, while the pseudostates $j = 6, ..., 15$ are approximated with the same accuracy and localized outside the well. The matrix elements between the bound states are localized in the vicinity of the barriers and the matrix elements between the pseudostates are localized beyond the barriers. The matrix elements between the bound states and pseudostates are small. The expansion of the desirable solution (5) over such orthogonal basis at ($j_{max} = 15$) with only ten closed channels taken into account allows the calculation of approximate solutions of the original 2D problem (2) at $E < 0$ with the required accuracy of h^{p+1} for the eigenfunctions and h^{2p} for the eigenvalues with respect to the maximum step h of the finite-element grid, p being the order of approximation. The solutions of the BVPs (6)-(12) were performed on the finite-element grids $\Omega_r = \{0(N_{elem} = 800)12\}$, and $\Omega_y = \{-12(N_{elem} = 120)12\}$, respectively, with N_{elem} fourth-order Lagrange elements $p = 4$ between the nodes, using the program KANTBP 3.0.[15]

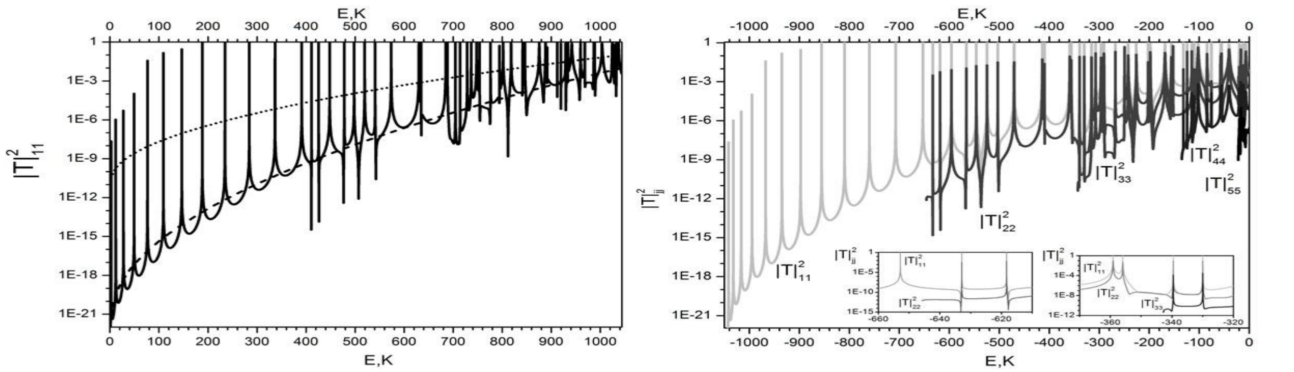

Figure 3. Left panel: Comparison of the total probability of penetration from the first channel to all five open channels simulated by the Galerkin expansion and Numerov calculations ; dotted and dashed curves are probabilities of penetration of one particle through one barrier and one particle through a sequence of two barriers, i.e., upper and lower average, respectively. Right panel: The total probability of penetration from the first channels with the energies $E_1 = -1044.879649$, $E_2 = -646.1570935$, $E_3 = -342.7919791$, $E_4 = -134.7843058$, $E_5 = -22.13407384$ (in K) to all five open channels, simulated by the Galerkin expansion.

The left panel of Fig. 3 illustrates the comparison of the total probability of penetration from the first channel to all five open channels simulated by Galerkin expansion and Numerov calculations. One can see that the position of resonances calculated with accuracy of order of 10^{-6} by the Galerkin expansion and Numerov procedure (at steps $h_x = 0.05$, $h_y = 0.05$ with accuracy $< 10^{-3}$) are in good agreement, the difference in height is explained by the crudeness of the energy grid used in the latter case. Probabilities of penetration of one particle through one barrier, one particle through a sequence of two barriers, and one particles with double mass through one barrier give approximations of upper, lower and average estimations. In the right panel of Fig. 3 we show the resonance behavior of the total probability of penetration with the transition from the first channels with the energies $E_1 = -1044.879649$, $E_2 = -646.1570935$, $E_3 = -342.7919791$, $E_4 = -134.7843058$, $E_5 = -22.13407384$ (in K) to all five open channels, simulated by the Galerkin expansion. The total transmission probability is seen to demonstrate the resonance behavior. Some peaks are high and narrow, and the position of peaks corresponding to transitions from different bound states are similar. As the energy of the initial excited state increases, the transmission peaks demonstrate a shift towards higher energies, the set of peak positions keeping approximately the same as for the transitions from the ground state and the peaks just replacing each other, like it was observed in the model calculations.[16] For example, the left epure shows that the positions of the 13th and 14th peaks for transitions from the first state coincide with the positions of the 1st and 2nd peaks for the transitions from the second state, while the right epure shows that the positions of the 25th and 26th peaks for transitions from the first state coincide with the positions of the 13th and 14th peaks for transitions from the second state and with the positions of the 1st and 2nd peaks for the transitions from the third state.

One can suppose that a better fit of the Morse potential to the observable upper part of the discrete spectrum of Be molecule, containing six more Val der Waals bound states, will increase the density of peaks near the dissociation threshold.[17–20] As one can see from right panels of Fig. 2, the diagonal potentials $V_{jj}(y)$ have shapes of double barriers and nondiagonal matrix elements V_{ij} have size less then four time. It means that positions of peaks are real part of energy of the quasistationary states imbedded in continuum that are predominately localized between double barriers. It is confirmed by behavior of probability density of coefficient functions $\chi_{ji_o}(y)$. The examples from Fig. 4 shows that in the case of resonance transmission the wave functions, depending on the center-of-mass variable y, are localized in the vicinity of the potential barrier center ($y = 0$), and in the case of total reflection the wave functions are localized at the barrier side, on which the wave is incident, and decrease to zero within the effective range of the barrier action. For the energy values, corresponding to some of the transmission coefficient peaks in Fig. 3 at within the effective range of barrier potential action the wave functions demonstrate considerable increase (till 10^6 times, see Fig. 4) of the probability density in comparison with the incident unit flux. This is a fingerprint of quasistationary states, which is not a quantitative definition, but a clear evidence in favour of their presence in the system.[21, 22]

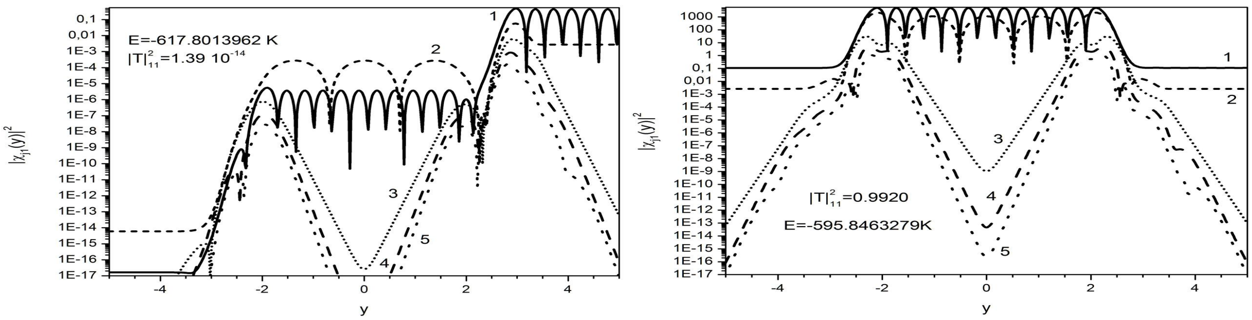

Figure 4. The examples of probability $|\chi_{j1}(y)|^2$ of component of vector-functions in the case of total reflection (left) and resonance transmission (right).

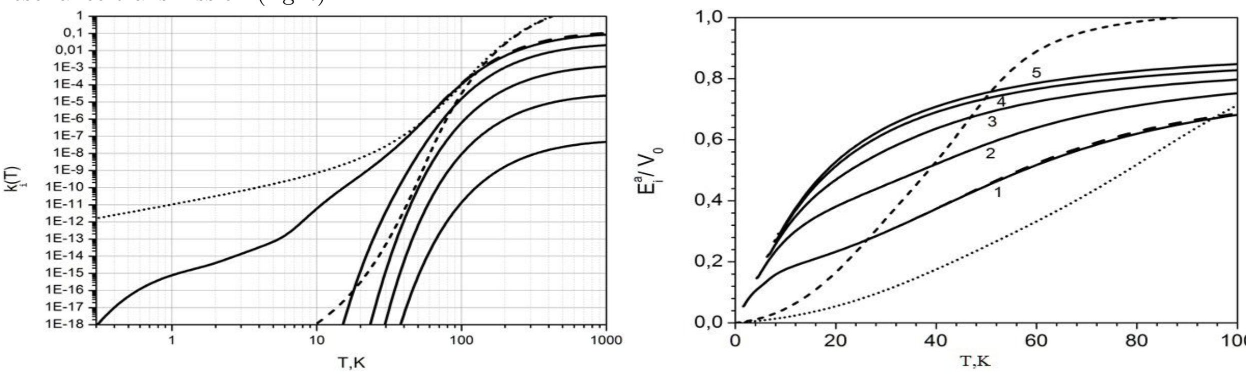

Figure 5. Left panel: Thermal rate constants vs. temperature: partial $k_i(T)$ (solid curve) and total $\hat{k}(T)$ (dashed lines) and their upper (dotted curves) and lower (short dashed) estimations. Right panel: The temperature-dependent activation energy: partial $E_i^a(T)$ (solid curve) and total $E^a(T)$ (dashed lines) activation energy, and its approximation of lower (dotted curves) and upper (short dashed) estimations that produced by corresponding upper and lower estimations of $k(T)$ of the left panel.

For a quantum particle, the possibility of tunneling makes the concept of activation barrier ill defined and therefore deviations from Arrhenius behavior may be expected. Normalized total thermal rate constant $\hat{k}^{qn}/k^{qn}_{(0)}$ have of the form:[4, 23]

$$\hat{k}^{qn}/k^{qn}_{(0)} = \sum_{i=1}^{N_o} \hat{k}_i(T), \quad \hat{k}_i(T) = \frac{e^{-\tilde{\varepsilon}_i/T}}{Q_{vib}} k_i(T), \quad Q_{vib} = \sum_{i=1}^{N_o} e^{-\tilde{\varepsilon}_i/T}, \tag{13}$$

$$k_i(T) = \frac{1}{\sqrt{T}} \int_0^{\tilde{E}_y^{\max}} W_{ii}(\tilde{E}_y) e^{-\tilde{E}_y/T} d\tilde{E}_y + \frac{1}{\sqrt{T}} \int_{\tilde{E}_y^{\max}}^{\infty} W_{ii}(\tilde{E}_y) e^{-\tilde{E}_y/T} d\tilde{E}_y. \tag{14}$$

where $\hat{k}_i(T)$ are weighed thermal rate constants, Q_{vib} is vibrational energy counted of the bottom of the Morse potential and $k_i(T)$ is partial thermal rate constant in initial vibrational state i, $W_{ii}(\tilde{E}) = |T|^2_{ii}(\tilde{E})$ is the total transmission probability for initial state i. Fig. 5a displays the comparison of partial $k_i(T)$ and total $\hat{k}(T)$ thermal rate constant vs temperature T and with their upper and lower estimations. Diffusion can still be approximately described by using a temperature-dependent activation energy, often much lower than the classical energy barrier. The temperature-dependent activation energy: total $\hat{E}^a(T)$ and partial $E_i^a(T)$ are defined by

$$\hat{E}^a(T) = -\frac{1}{\sqrt{\beta}\hat{k}(T)} \frac{d\sqrt{\beta}\hat{k}(T)}{d\beta}, \quad E_i^a(T) = -\frac{1}{\sqrt{\beta} k_i(T)} \frac{d\sqrt{\beta} k_i(T)}{d\beta}, \quad \beta = 1/T.$$

Fig. 5a displays the comparison of partial $E_i^a(T)$ and total $\hat{E}^a(T)$ activation energy vs temperature T and with their upper and lower estimations in restricted interval till $T_{\max} = 100K$. So, activation energy E^a for a composite system less then two noninteracted particles. With increasing temperature T contribution of high energies E_y, will be taking into account.

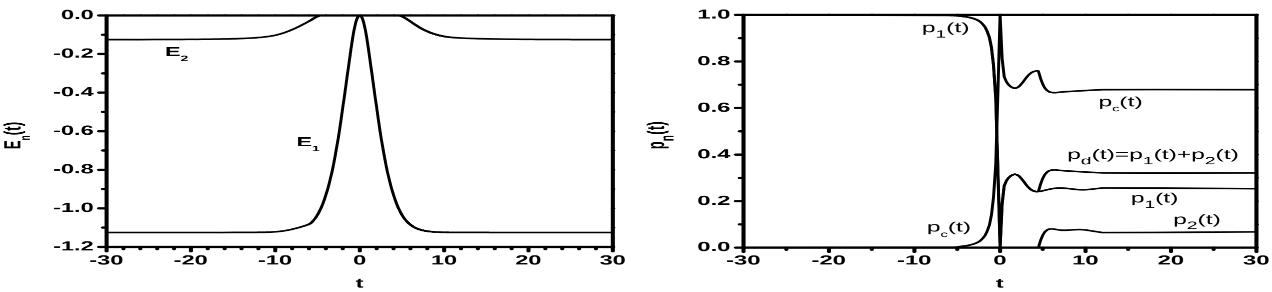

a) b)

Figure 6. a) Eigenenergies $E_n(t)$ of the instant Hamiltonian depending on time as a parameter t. b) The bound state probabilities $p_1(t)$, $p_2(t)$ and the ionization probability $p_c(t)$ versus the time t. Here $A_0 = -15/8$, $A_1 = 15/8$, $v = 1/2$, $x_0(t_0) = vt_0 = -15$, and $t_0 = -30$.

3. MODEL II. IONIZATION OF A PÖSCHL-TELLER ATOM

Let us consider simplified model of collision of antiproton ($\bar{p}$+H) or proton (p+H) on hydrogen atom where incident nucleus moves by straight line classical trajectory with the velocity v, which describe by the TDSE on the finite time interval $t \in [t_0, T]$ for the two-center problem[24] with Pöschl-Teller potentials, similar to the ionization problem.[25] We consider a particular case of a resting well, $A_0 < 0$, and a barrier, $A_1 > 0$, (or a well at $A_1 < 0$) moving with the velocity v with respect to the resting well in units $\hbar = m_e = 1$:

$$\imath \frac{\partial \psi(x,t)}{\partial t} = H(x,t)\psi(x,t),$$
$$H(x,t) = -\frac{1}{2}\frac{\partial^2}{\partial x^2} + \frac{A_0}{\cosh^2(x)} + \frac{A_1}{\cosh^2(x - x_0(t))}, \tag{15}$$

where $H(x,t)$ is the instant Hamiltonian and $x_0(t) = vt$ is the position of the moving barrier center. For numerical calculation **with required accuracy** the initial infinite-axis boundary problem is reduced to a sufficiently large finite interval $x \in (x_{\min}, x_{\max})$ with the boundary and normalization conditions

$$\psi(x_{\min}, t) = 0, \quad \psi(x_{\max}, t) = 0, \quad \|\psi(x,t)\|^2 = \int_{x_{\min}}^{x_{\max}} |\psi(x,t)|^2 dx = 1. \tag{16}$$

We consider an example of the wave packet evolution in the time interval $t \in [t_0, T]$, induced by the barrier ($A_1 = 15/8$) moving with the velocity v with respect to the motionless well ($A_0 = -15/8$) that supports two bound states $n_0 = 2$ with the energies $E_1(t = t_0) \cong E_1^W = -9/8 = -1.125$ and $E_2(t = t_0) \cong E_2^W = -1/8 = -0.125$.

For $v > 0$ we choose the initial time t_0 and the final time T to correspond to the initial $x_0(t_0) = vt_0 = -15$ and the final $x_0(T) = vT = 15$ positions of the moving barrier center with the aim to preserve with required accuracy the discrete spectrum states supported by the resting well at both t_0 and T. We start from the initial state that corresponds with required accuracy to the ground state supported by the resting well

$$\psi(x, t_0) \cong \psi_1^W(x) = N_1(\cosh x)^{-(\sqrt{1-8A_0}-1)/2}. \tag{17}$$

Note that in the case $A_1 + A_0 = 0$ at $t = 0$ the potential of the problem (15) is equal to zero on the entire axis and the instant Hamiltonian $H(x,t)$ at $t = 0$ has purely continuous spectrum that provides the complete ionization of the considered quantum system and the capture to the discrete spectrum states during further evolution.

The calculations were performed using the program TIME6T[26] within the spatial interval $x \in (-512, 512)$, which was sufficient to avoid reflection from the boundaries within the considered time interval $t \in [t_0, T]$. The wave functions $\psi_n(x;t)$ of the discrete spectrum $E_n < 0$ and the wave functions $\psi_E^\nu(x;t) \equiv \psi_{\overleftrightarrow{E}}(x;t)$ of the continuous spectrum $E \geq 0$ of the instant Hamiltonian $H(x,t)$ depend on t as a parameter, as follows from Eq.

(15). They were calculated in the spatial interval $x \in (x_{\min}, x_{\max})$ with the homogeneous third-type boundary conditions by mean of the modified[15] KANTBP program[12] using the appropriate asymptotic expressions. The subscript ν equals $\rightarrow$ or $\leftarrow$ for the positive or negative direction of the final momentum $q = \pm\sqrt{2E}$, respectively. After joining the asymptotic expressions on the entire axis $x \in (-\infty, +\infty)$, these functions satisfy the conventional relations

$$\int_{-\infty}^{+\infty} dx (\psi_E^{\nu'}(x;t))^* \psi_{E'}^{\nu}(x;t) = (2\pi)\delta(E - E')\delta_{\nu\nu'}, \tag{18}$$

$$\int_{-\infty}^{+\infty} dx (\psi_E^{\nu}(x;t))^* \psi_n(x;t) = 0, \tag{19}$$

$$\sum_{n=1}^{n_0} \psi_n(x;t)\psi_n(x';t) + \sum_{\nu=\rightleftarrows} \int_0^{+\infty} dE (\psi_E^{\nu}(x;t))^* \psi_E^{\nu}(x';t) = \delta(x - x'). \tag{20}$$

An example of the dependence of eigenenergies $E_n < 0$ of the instant Hamiltonian upon the time parameter t is shown in Fig. 6a. In the vicinity of $t = 0$ the Hamiltonian is seen to have only one eigenvalue $E_1 < 0$ and at $t = 0$ it has only a continuous spectrum.

The probabilities $p_n(t)$ and $p_c(t)$ of transitions to the bound and continuum states and the energy distribution of probability $p_E(t)$ in the continuous spectrum $E \geq 0$ in the above capture and ionization processes are calculated using the expressions

$$p_n(t) = |t_{n0}(t)|^2, \quad t_n(t) = \int_{x_{\min}}^{x_{\max}} dx (\psi_n(x,t))^* \psi(x,t) \tag{21}$$

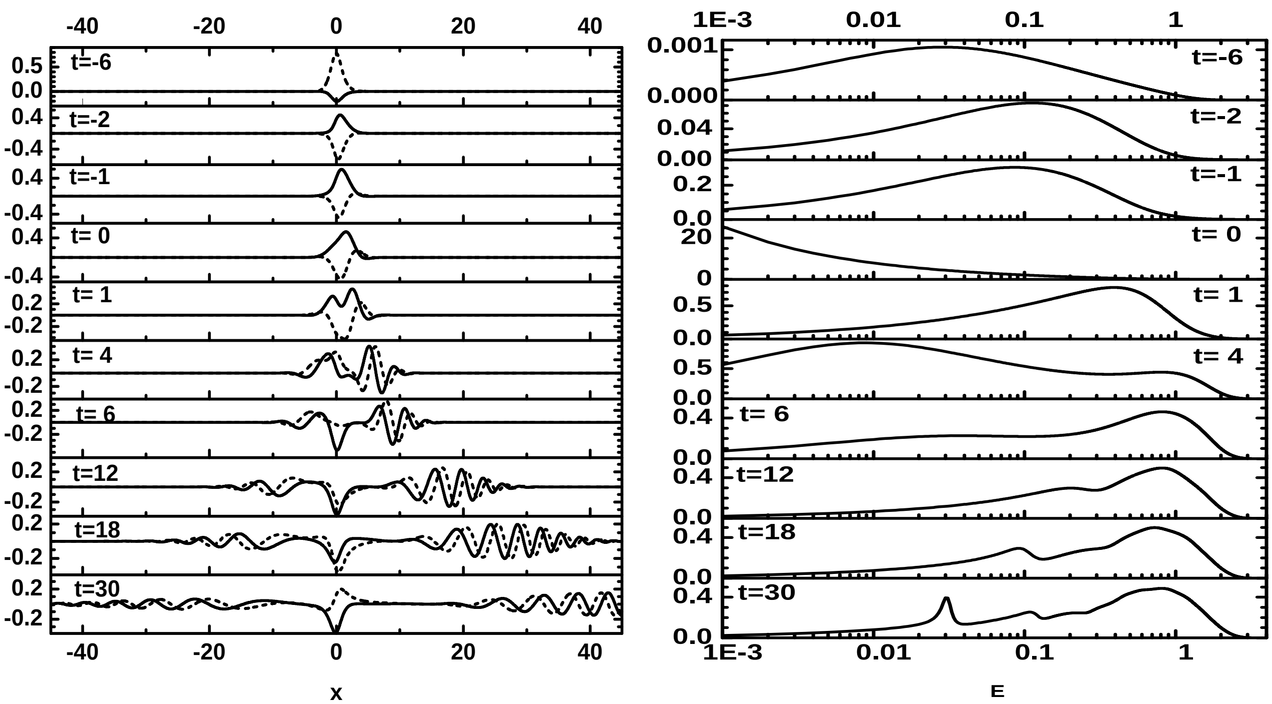

a) b)
Figure 7. a) The real part (solid line) and the imaginary part (dashed line) of the wave function; b) the energy distribution of ionization probability $p_E(t)$ at different moments of time t for the fixed values of parameters $v = 1/2$, $A_0 = -15/8$, $A_1 = 15/8$ and the initial position of the moving barrier $x_0(t_0) = vt_0 = -15$, $t_0 = -30$.

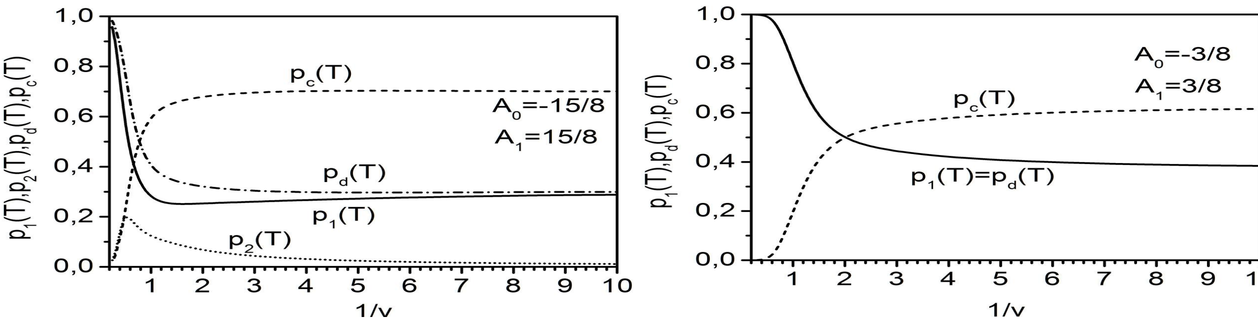

Figure 8. The probabilities $p_1(T)$, $p_2(T)$ of the ground state and lower excited states, and the ionization probability $p_c(T)$ versus the inverse velocity $1/v$ for the time $T = 15/v$ and the initial time $t_0 = -15/v$, when the position of the center of barrier is $x_0(T) = 15$ and $x_0(t_0) = -15$, respectively.

$$p_E(t) = \frac{|t_E^{\rightarrow}(t)|^2 + |t_E^{\leftarrow}(t)|^2}{2\pi}, \quad t_E^{\overleftrightarrow{}}(t) = \int_{x_{\min}}^{x_{\max}} dx (\psi_E^{\overleftrightarrow{}}(x,t))^* \psi(x,t). \tag{22}$$

As follows from Eq. (20), they satisfy with the required accuracy the condition at $E_{\max} \gg 1$:

$$\sum_{n=1}^{n_0} p_n(t) + p_c(t) = 1, \quad p_c(t) = \int_0^{E_{\max}} p_E(t) dE. \tag{23}$$

As mentioned above, at $t = 0$ the effective potential is zero, and the eigenfunctions of the instant Hamiltonian correspond to the continuous spectrum. Then the effective potential becomes nonzero again and the capture to the exited and ground states become possible, which is seen from the evolution of probabilities $p_E(t)$ and $p_c(t)$ in Figs. 6b and 7. Fig. 7 shows that at $t \geq 1$ the maxima of the energy distribution $p_{E\sim 1} \sim 0.5$ correspond to the forward and backward ionization waves with similar frequencies. The maxima of $p_c(t)$ at $t \sim 4$ in Fig. 6b correspond to the maxima of $p_{E\sim 0.01} \sim 1$ at $t = 4$ in Fig. 7b and correlate with ionization and capture processes. With increasing velocity the probability densities of the excited states tend to zero (see Fig. 8). The

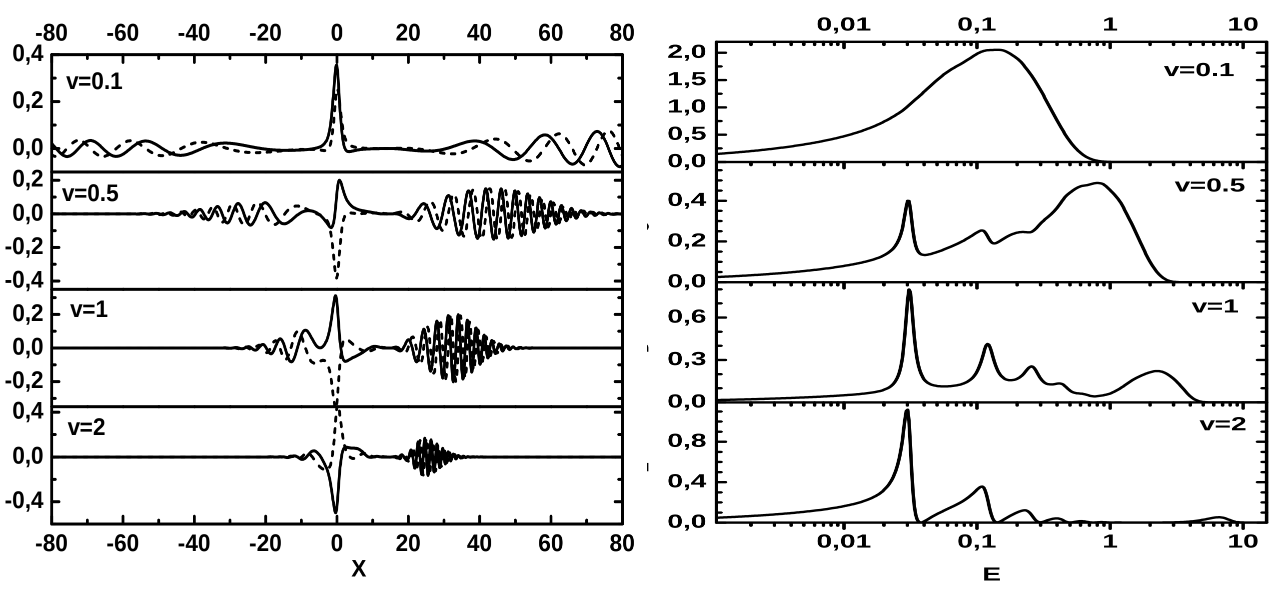

a) b)

Figure 9. a) The real part (solid line) and the imaginary part (dashed line) of the wave function; b) the energy distribution of ionization probability $p_E(T)$ for the fixed velocity values $v = 0.1, 0.5,\ 1,\ 2$ at $A_0 = -15/8$, $A_1 = 15/8$.

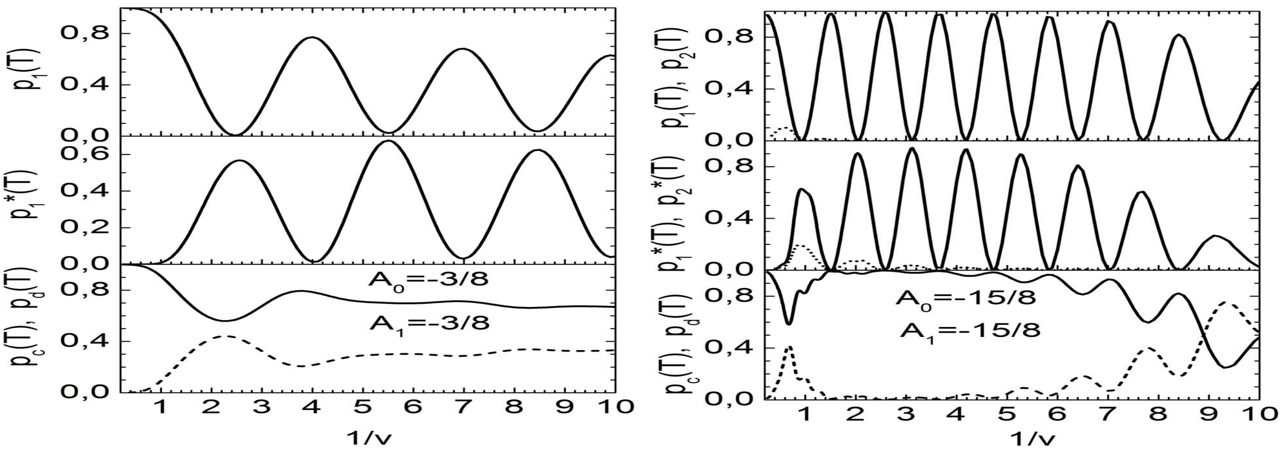

Figure 10. The probabilities $p_1(T)$, $p_2(T)$ of the ground and lower excited states in a resting well, the probabilities $p_1^*(T)$, $p_2^*(T)$ of the ground and lower excited states in a moving well, and the ionization probability $p_c(T)$ versus the inverse velocity $1/v$ for the time $T = 15/v$ and the initial time $t_0 = -15/v$, when the position of the barrier center is $x_0(T) = 15$ and $x_0(t_0) = -15$, respectively.

wave function and the distribution of ionization probability $p_E(t)$ for some particular values of the velocity are shown in Fig. 9. As seen from Fig. 9, with increasing v the forward ionization waves become dominant and their energy increases.

Consider another example of the evolution of the wave packet in the time interval $t \in [t_0, T]$, induced by the barrier ($A_1 = 3/8$) moving with the velocity v with respect to the fixed well ($A_0 = -3/8$), supporting a single bound state $n_0 = 1$ with energy $E_1(t = t_0) \cong E_1^W = -1/8 = -0.125$. Fig. 8 shows that, generally, the velocity distribution of the probability has the similar structure. Note, that the probability of detecting the system in the excited states is substantially smaller than that in the ground state.

For two cases discussed above let us consider an example of the wave packet evolution, induced by the well

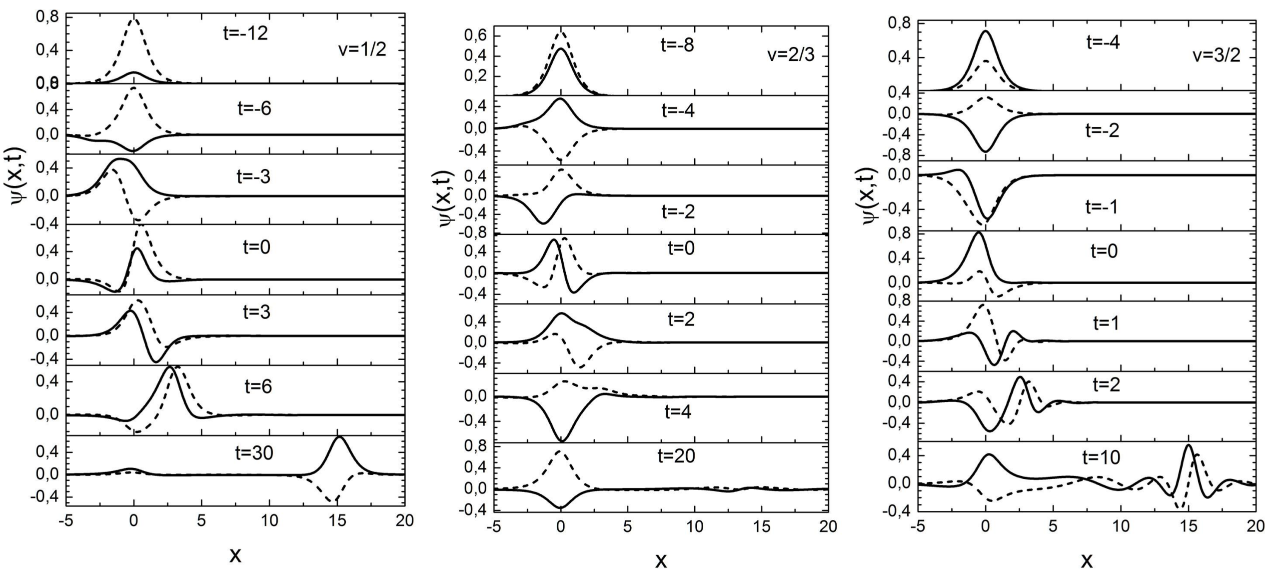

a) b)

Figure 11. a) The real part (solid line) and the imaginary part (dashed line) of the wave function for three fixed values of velocity $v = 1/2, 2/3, 3/2$ at different moments of time t and $A_0 = A_1 = -15/8$.

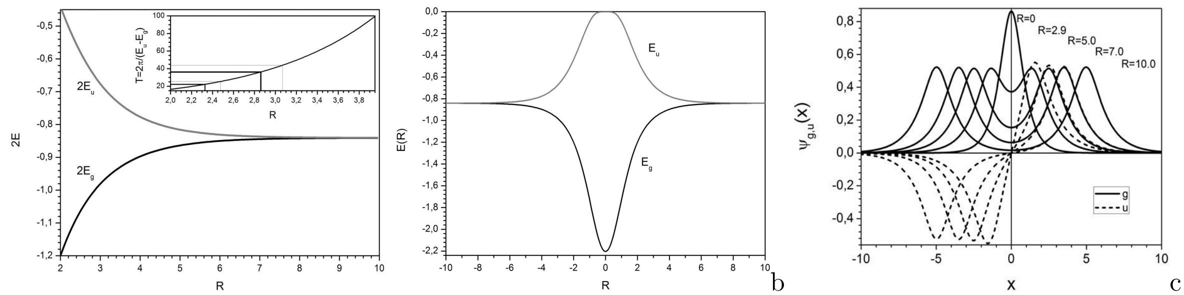

Figure 12. The potential curves (a,b) and the wave functions (c) of the ground (gerade g) and excited (ungerade u) states of the electron at different values of the internuclear distance R. The inset in Fig. (a) shows the dependence of the free oscillation period upon R. The values of R corresponding to the maxima of ionization probability are shown by vertical lines.

($A_1 = A_0$), moving with the velocity v, in the time interval $t \in [t_0, T]$. An example of the dependence of eigenenergies $E_n < 0$ and eigenfunctions of the instant Hamiltonian, having also a continuous spectrum, upon the time parameter t is shown in Fig. 12b,c as a function of $R = vt$. At $t = 0$, i.e. at $R = 0$, the Hamiltonian is seen to have only one eigenvalue $E_1(R = 0) < 0$ because in this point $E_2(R = 0) = 0$, i.e. second eigenvalue touch boundary of continuous spectrum and after that go to unphysical sheet of energy. At $t > 0$ the bound state corresponding second eigenvalue appears again and its settlement occurs by capture of ionized particles to discrete spectrum $E_2(R \neq 0) < 0$. Fig. 10 shows the dependence of probabilities $p_1(T)$, $p_2(T)$ of detecting the system in the ground and first excited states in the resting well and the probabilities $p_1^*(T)$, $p_2^*(T)$ for the ground and first excited states in the moving well versus the inverse velocity $1/v$. The Figure 10 shows that the probability to remain in the resting well or to go to the moving one is rapidly oscillating at small v, which is due to multiple reflection of the wave packet from the walls of the wells. The probability of transition to the continuum is also a rapidly oscillating functions at $v \to 0$, due to the reflection from the walls of the wells. There is also a peak at $v \sim 0.5$ in the case of $A_0 = -3/8$ and at $v \sim 1.5$ in the case of $A_0 = -15/8$, which are associated with the appearance of the barrier, separating the wells starting from the time $t = \ln(2 + \sqrt{3})/v$.

Figure 11 shows the time dependence of the wave function $\psi(x, t)$ at the velocities of the well $v = 1/2$, $v = 2/3$, and $v = 3/2$, when the wave packet passes to the moving well, remains localized in the resting well, and is partially converted into the continuum, respectively. At low velocities the wave packet is seen to oscillate. At high velocities the mutual influence of the wells becomes negligible, and in the limit $v \to \infty$ the scattering becomes purely elastic.

The considered models allow the description of composite systems in transient effective potentials that may cause not only the excitation and ionization processes, but also the capture to bound states. The models are advantageous for demonstrating the efficiency of computational unitary schemes, implemented in the applied program TIME6.

4. MODEL III. IONIZATION DYNAMICS OF A MOLECULAR ION

Now consider a simplified one-dimensional model of molecular ion with two nuclei fixed at the points $\pm R/2$, attracting an electron at the point x via a superposition of two identical PöschlTeller (PT) potentials. The system is affected by the electric field of a laser pulse. The Scrödinger equation describing the ionization dynamics of this model (in atomic units) reads

$$
\begin{aligned}
&\imath \frac{\partial \psi(x,t)}{\partial t} = H(x,t)\psi(x,t), \qquad (24)\\
&H(x,t) = H_0(x) + V(x,t)\\
&H_0(x) = -\frac{1}{2}\frac{\partial^2}{\partial x^2} - \frac{V_0}{\cosh^2((x - R/2)/L)} - \frac{V_0}{\cosh^2((x + R/2)/L)},
\end{aligned}
$$

Here $V(x,t)$ is the potential induced by the laser pulse

$$V(x,t) = F_0 f(t)\sin(\omega_L t), \tag{25}$$

with the amplitude F_0 and the frequency ω_L. We choose the envelope function $f(t)$ of the laser pulse in the form $f(t) = \sin^2(\pi t/T_{pulse})$, where T_{pulse} is the pulse duration.

The BVP for Eq. (24) was solved with the boundary and normalization conditions (16) and the initial state $\psi(x,0) = (\psi_g + \psi_u)/\sqrt{2}$ localized in the right-hand well of the double-well potential. The finite spatial interval $x \in (-128, 128)$ was sufficient to avoid reflection from the boundaries within the considered time interval $t \in [t_0, T]$ using the program TIME6T.[26]

Figures 12–15 present the results of calculations performed using the following parameters. The magnitude and the width of the PT potentials were $V_0 = 2.216E_h$ and $L = 2/3a_B$, respectively, where $E_h \equiv Ry = \hbar^2/2/m_e/a_B$ and $a_B = \hbar^2/m_e/e^2$ is the Bohr radius. The laser frequency $\omega_L = 0.16546$ corresponded to the wavelength $\lambda = 300$ nm and the period $T_{oc} = 2\pi/\omega_L = 37.973$; the pulse duration was taken to be $T_{pulse} = 32T_{oc}$.

For the fixed values of the parameter $R > R_0 \approx 0.1$ the Hamiltonian $H_0(x;R)$ has two eigenvalues, corresponding to the ground and excited state that vary with the distance between wells as shown in Fig. 12a. The eigenstates possess the symmetry with respect to permutations of identical nuclei, namely, the ground state is even (gerade, g) and the excited state is odd (ungerade, u). With respect to the center of symmetry the wave function is symmetric for g state and antisymmetric for u state. The wider is the barrier, the smaller is the separation between the energy levels. In the process of evolution, the wave function of the initial state $\psi_a(x) = (\psi_g + \psi_u)/\sqrt{2}$ localized in the well (a) turns into the the wave function $\psi_b(x) = (\psi_g - \psi_u)/\sqrt{2}$, localized in the well (b), and then returns to the initial state. In the absence of external fields the evolution of the initial state $\psi(x,0) = \psi_a(x)$ (Fig. 13 at $R = 2.9$) can be described by the formula

$$\begin{aligned}\psi(x,t) &= \frac{1}{2}(\psi_g(t) + \psi_u(t)) = \frac{1}{2}(\psi_g \exp(iE_g t) + \psi_u(t)\exp(iE_u t))\\ &= \frac{\exp(iE_g t)}{2}[\psi_a(x)(1+\exp(i(E_u - E_g)t) + \psi_b(x)(1-\exp(i(E_u - E_g)t)].\end{aligned}$$

The period of free oscillation $T \equiv T_{gu} = 2\pi/(E_u - E_g)$ versus the distance R is shown in the inset of Fig. 12a. At $R = 2.9$ the frequency of free oscillation is equal to the wave frequency.

In Fig. 14 the probability P_+ of the particle localization in the right-hand well and the total discrete spectrum probability P at $T_{fin} = 36T_{oc}$ are shown as functions of R (left) and the free oscillation frequency ω_{gu} (right).

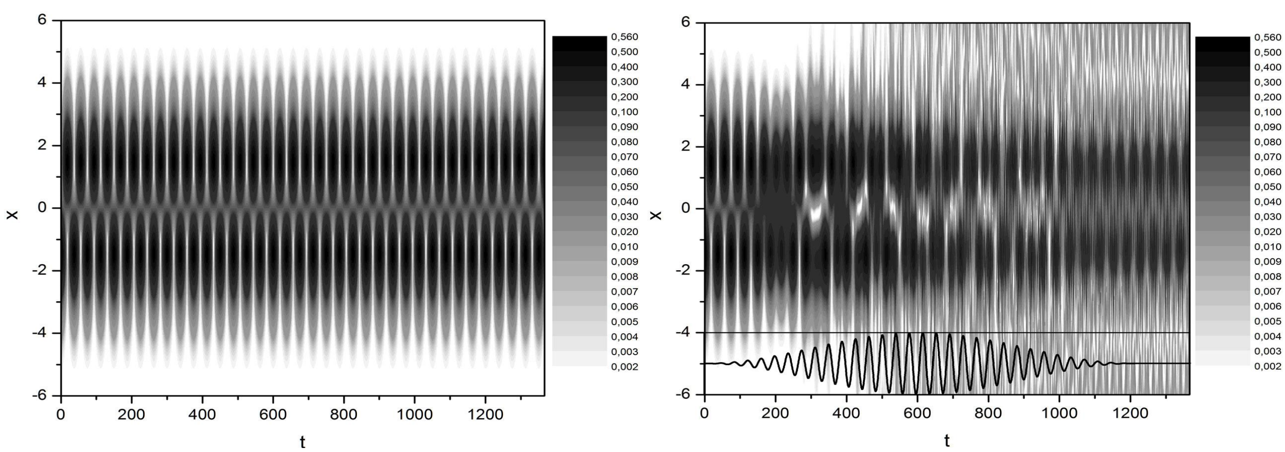

Figure 13. Temporal dynamics of the wave function without the laser pulse (left) and with the laser pulse (right). $R = 2.9$, the line plots the laser pulse $f(t)\sin(\omega_L t)$, $\omega_L = 0.16546$, $F_0 = 0.05$ a.u. Note that the laser frequency is close to the resonance 1:1, i.e. $\omega_L = \omega_{gu}$.

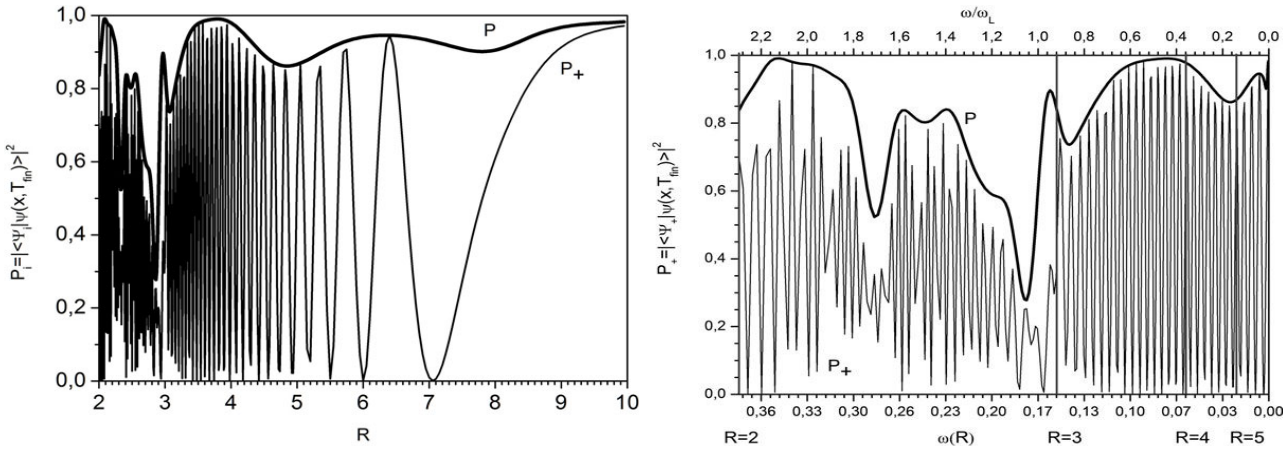

Figure 14. The probability P_+ of the particle localization in the right-hand well and the total discrete spectrum probability P at the time $T_{fin} = 36T_{oc}$ as functions of the internuclear distance R (left) and the free oscillation frequency ω (right).

From Fig. 14 the probability of electron localization in the initial state $\psi_a(x, T_{fin})$ at the moment of time T_{fin} at $R \ll 10$ is seen to be a fast oscillating function of R. The total discrete spectrum probability P is a slow varying function everywhere except the interval $R \in (2.2, 4.2)$, in which P has four peaks. These peaks are clearly seen in the right panel of Fig. 14. The values of R corresponding to the resonance periods T_{gu} and frequencies ω_{gu} are indicated by straight lines in the inset of Fig. 12a. The greatest peak is located in the vicinity of $R \approx 2.86$ for which the free oscillation frequency $\omega_{gu} \approx 0.173$ ($T_{gu} \approx 36.2$) is approximately equal to the laser pulse frequency $\omega_L = 0.16546$, $\omega_{gu} \approx \omega_L$, and the second peak is located at $R \approx 2.33$, for which the free oscillation frequency $\omega_{gu} \approx 0.282$ ($T_{gu} \approx 22.2$) is approximately by 3/2 times larger than ω_L, $\omega_{gu}/\omega_L \approx 3/2$. Thus, the resonances $1:1$ (the evolution of which is shown in Fig. 13) and $3:2$ are observed, the small deviations being due to the small pulse duration and the variation of its envelope.

The time dependence of the probability P_+ of the particle localization in the right-hand well and of the total

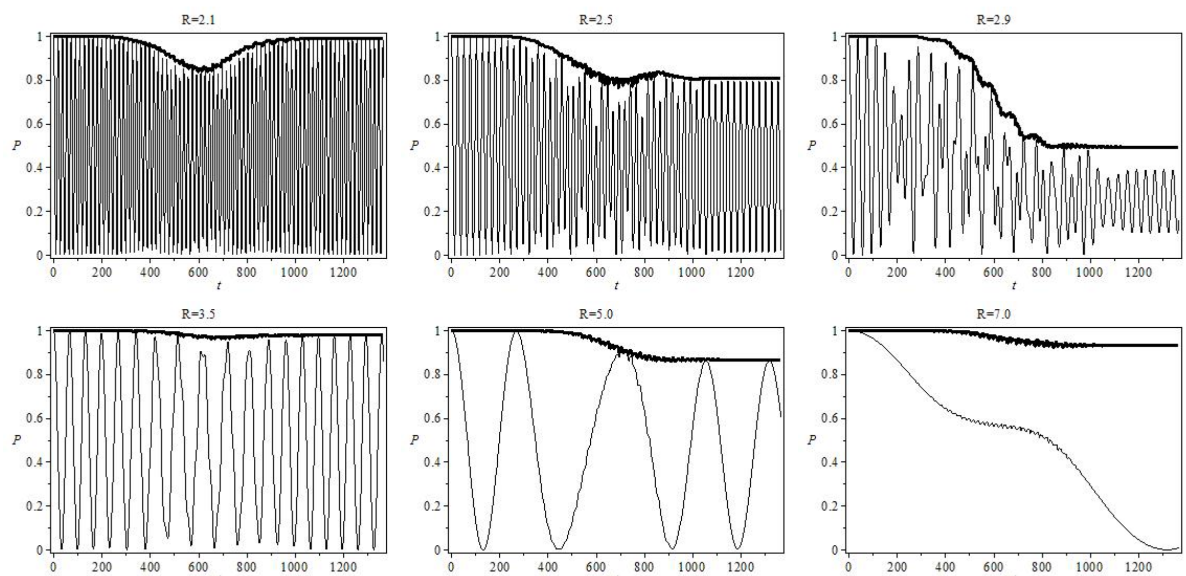

Figure 15. The probability P_+ of the particle localization in the right-hand well and the total discrete spectrum probability P as functions of time t at different values of R.

discrete spectrum probability P at different values of R is shown in Fig. 15. It is seen that at large distance between the wells the period of free oscillation is large, and the ionization occurs from a definite well. Decreasing the separation between the wells gives rise to the additional resonance ionization when the resonance frequency conditions are satisfied and the capture form the continuum otherwise.

5. CONCLUSIONS

The effect of quantum transparency in resonance tunneling of diatomic molecules through repulsive potential barriers is demonstrated and shown to lead to quantum diffusion by the example of diatomic low-dimensional model systems, coupled via realistic molecular potentials. The proposed models and approach, the quantum transparency effect itself and the developed software can find further applications in barrier heavy-ion reactions and molecular quantum diffusion. They can be also applied in the studies of laser control of molecular tunneling, aimed at enhancing the rate of chemical reactions and quantum diffusion.

5.1 Acknowledgments

The work was supported partially by grants RFBR14-01-00420 and 13-01-00668, 13-602-02 JINR and 0602/GF MES RK. Authors thank profs. F.M. Penkov and A.V. Mitin for collaboration.

REFERENCES

[1] Pen'kov, F.M., "Quantum transmittance of barriers for composite particles," JETP 91, 698–705 (2000).

[2] Pen'kov, F.M., "Metastable states of a coupled pair on a repulsive barrier," Phys. Rev. A 62, 044701–1–4 (2000).

[3] Shotter, A.C. and Shotter, M.D., "Quantum mechanical tunneling of composite particle systems: Linkage to sub-barrier nuclear reactions," Phys. Rev. C 83, 054621–1–11 (2011).

[4] Pijper, E. and Fasolino, A., "Quantum surface diffusion of vibrationally excited molecular dimers," J. Chem. Phys. 126, 014708–1–10 (2007).

[5] Kavka, J.J., Shegelski, M.R.A. and Hong, W.P., "Tunneling and reflection of an exciton incident upon a quantum heterostructure barrier," J. Phys.: Condens. Matter. 24, 365802–1–13 (2012).

[6] Shegelski MRA, Hnybida J., Vogt R. "Formation of a molecule by atoms incident upon an external potential," Phys.Rev. A. 78, 062703–1–5 (2007).

[7] Bondar, D.I., Liu, W.-Ki, Ivanov, M.Yu., "Enhancement and suppression of tunneling by controlling symmetries of a potential barrier," Phys. Rev. A 82, 052112–1–9 (2010).

[8] Gusev, A., Vinitsky, S., Chuluunbaatar, O., Rostovtsev, V.A., Hai, L.L., Derbov, V. and Krassovitskiy, P., "Symbolic-numerical algorithm for generating cluster eigenfunctions: tunneling of clusters through repulsive barriers," Lecture Notes in Computer Science 8136, 427–442 (2013).

[9] Gusev, A.A., Vinitsky, S.I., Chuluunbaatar, O., Gerdt, V.P., Rostovtsev V.A., "Symbolic-numerical algorithms to solve the quantum tunneling problem for a coupled pair of ions," Lecture Notes in Computer Science 6885, 175–191 (2011).

[10] Shapiro, M. and Brumer, P., [Quantum Control of Molecular Processes] Wiley-VCH, Weinheim, 2012.

[11] Chuluunbaatar, O., Gusev, A.A., Vinitsky, S.I. and Abrashkevich, A.G., "A program for computing eigenvalues and eigenfunctions and their first derivatives with respect to the parameter of the parametric self-adjoined Sturm-Liouville problem", Computer Physics Communications, 180, 1358-1375 (2009).

[12] Chuluunbaatar, O., Gusev, A.A., Vinitsky, S.I. and Abrashkevich, A.G., "KANTBP 2.0: New version of a program for computing energy levels, reaction matrix and radial wave functions in the coupled-channel hyperspherical adiabatic approach," Comput. Phys. Commun. 179, 685–693 (2008).

[13] Fundamental Physical Constants http://physics.nist.gov/constants

[14] Lauhon, L.J. and Ho, W., "Direct observation of the quantum tunneling of single hydrogen atoms with a scanning tunneling microscope," Phys. Rev. Lett. 85, 4566–4569 (2000).

[15] "A program package for solution of two-dimensional discrete and continuum spectra boundary-value problems in kantorovich (adiabatic) approach," Program library "JINRLIB" http://wwwinfo.jinr.ru/programs/jinrlib/kantbp/indexe.html

[16] Ahsan, N., and Volya, A., "Quantum tunneling and scattering of a composite object reexamined," Phys. Rev. C 82, 064607–1–19 (2010)

[17] Merritt, J.M., Bondybey, V.E. and Heaven, M.C., "Beryllium Dimer — Caught in the Act of Bonding" Science 326, 1548–1551 (2009).

[18] Patkowski, K., Špirko V., and Szalewicz, K. "On the Elusive Twelfth Vibrational State of Beryllium Dimer" Science 326, 1382–1384 (2009).

[19] Mitin, A. V., "Accurate calculations of dissociation energies of weakly bonded He_2 and Be_2 molecules by MRCI method," Russ. J. Phys. Chem. A. 84, 2314–2319 (2010).

[20] Mitin, A. V., "Ab initio calculations of weakly bonded He_2 and Be_2 molecules by MRCI method with pseudo-natural molecular orbitals," Int. J. Quantum Chem. 111, 2560–2567 (2011) .

[21] Baz', A.I., Zel'dovich, Ya.B. and Perelomov, A.M., [Scattering, Reactions, and Decay in Nonrelativistic Quantum Mechanics], Jerusalem, 1969; Nauka, Moscow, 1971.

[22] de Carvalho, C.A.A. and Nussenzveig, H.M., "Time delay," Phys. Rept. **364**, 83–174 (2002).

[23] Miller, W.H. "Quantum mechanical transition state theory and a new semiclassical model for reaction rate constants", J. Chem.Phys. 61, 1823–1834 (1974).

[24] Soloviev, E.A. and Vinitsky, S.I. "Suitable coordinates for the three-body problem in the adiabatic representation", J. Phys. B 18, L557-L562 (1985).

[25] Corso, P.P., Fiordilino, E. and Persico, F., "Ionization dynamics of a model molecular ion," J. Phys. B: At. Mol. Opt. Phys. 38, 1015–1028 (2005).

[26] Vinitsky, S.I., Gusev, A.A. and Chuluunbaatar, O., "Program complex for the numerical solution of the Cauchy problem for the time-dependent Schroedinger equation," Program library "JINRLIB" http://wwwinfo.jinr.ru/programs/jinrlib/time6t/indexe.html